RSC Advances

PAPER

View Article Online
View Journal | View Issue

Cite this: *RSC Adv.*, 2020, **10**, 7771

PPy nanoneedle based nanoplatform capable of overcoming biological barriers for synergistic chemo-photothermal therapy†

Yanyan Yin,[a] Yutong Hao,[b] Ning Wang,[b] Pengfei Yang,[a] Na Li,[a] Xiaoyi Zhang,[a] Yu Song,[a] Xuebing Feng[c] and Weiwei Ma*[a]

Received 2nd December 2019
Accepted 18th January 2020

DOI: 10.1039/c9ra09917d

rsc.li/rsc-advances

The biological barriers *in vivo* have limited the site-specific bioavailability and impeded therapeutic efficacy. To tackle these issues, nonspherical particles with a shape effect have attracted wide attention to affect the *in vivo* translocation of a drug delivery system. Herein, we constructed a nanoplatform based on polypyrrole (PPy) nanoneedles by hyaluronic acid (HA) modification and doxorubicin (DOX) loading. The PPy-HA@DOX nanoneedles with high aspect ratios could enhance the extravasation through the fenestrated vasculature of tumors, transport across tumor cell membrane *via* an endocytosis mechanism or even penetrated the membrane directly, and ultimately enter the nucleus easily *via* the nuclear pore complex by passive diffusion. With the ability of overcoming biological barriers, the PPy nanoneedle based nanoplatform would deliver drugs into the organelles more effectively. Under near infrared (NIR) laser irradiation, PPy as the photothermal agent could lead to tumor cellular structure damage for photothermal therapy (PTT). Therefore, PPy-HA@DOX developed here would exploit the merits of synergistic combination of chemo-photothermal therapy, which would pave the way toward more effective nanotherapeutics.

Introduction

In recent years, the advancement in nanomaterials has drawn widespread attention for biomedical applications, especially for cancer therapy.[1–4] In particular, the near infrared (NIR) resonant nanoparticles have developed rapidly in the past few years for cancer treatment.[5,6] Under NIR irradiation, the photothermal agents absorbed energy from photons and converted it into heat, leading to tumor cellular structure damage or apoptosis for photothermal therapy (PTT).[7–10] At present, various photothermal materials including carbon-based materials or metal nanostructures such as gold nanostructures, Pd nanosheets and silver nanoparticles were intensively investigated.[11–14] However, their poor photostability and potential toxicity hindered clinical application. By contrast, the organic conductive polymers, polypyrrole (PPy) nanoparticles, were an increasingly recognized alternative due to their excellent biocompatibility and photostability.[15–17] Besides, compared with most PTT agents, PPy NPs have higher photothermal conversion efficiency due to strong NIR absorbance.[18] Notwithstanding their potential, PPy nanoparticles faced a serious of biological barriers such as mononuclear phagocyte system, hemorheological flow limitations and endothelial extravasation, cellular internalization, nuclear drug delivery, and multidrug resistance, which limited the site-specific bioavailability and impeded therapeutic efficacy.[19,20]

To overcome these biological barriers, it was critical to design the nanomedicine.[21] It has been suggested that the shape effect due to the difference in curvature of nanoparticles could affect the hemorheological dynamics, cellular delivery and *in vivo* fate.[22–24] Compared to the size-matched spheres, the nonspherical particles exhibited seriously lateral drift, the unique tumbling and margination dynamics, which potentiated the propensity of nanoparticle-endothelial cell wall contact and then enhanced the extravasation through the fenestrated vasculature of tumors.[20] Furthermore, the rods or worms-shaped nanoparticles with high aspect ratios had larger contact area with the cell membrane than spherical nanoparticles, which could be internalized into the cells easily *via* endocytosis mechanism or even penetrated the membrane directly.[20,25] Similarly, the nanorods were inclined to enter nucleus *via* the nuclear pore complex by passive diffusion.[26] In this sense, it was highly desired to develop nonspherical particles capable of overcoming biological barriers. Interestingly, the PPy nanoneedles were investigated.[27,28] Benefiting from their unique needle-like morphology, PPy nanoneedles were expected to penetrate tumors more rapidly, and deliver drugs into the organelles more effectively.

[a]*School of Pharmacy, Xinxiang Medical University, Xinxiang 453003, China. E-mail: weiweima2019@163.com*

[b]*School of Pharmaceutical Sciences, Zhengzhou University, Zhengzhou 450001, China*

[c]*School of Stomatology, Shandong University, Jinan 250012, China*

† Electronic supplementary information (ESI) available. See DOI: 10.1039/c9ra09917d

According to several published protocols, the highly cationic PPy nanoneedles usually showed poor dispersibility and the short blood circulation property.[29] Thus, it is highly desired to introduce surface functional modification into the system. Hyaluronic acid (HA) as the extracellular matrix substance had been taken advantages in numerous biomedical applications.[30] With excellent hydrophilic character, HA modification endowed excellent stability of the system.[31] Notably, HA as a active tumor targeting ligand had high affinity with its CD44 receptor that over-expressed on various cancer cells.[32] On basis of this, the versatile HA modification should provide a multifunctional drug delivery system.

In this work, we constructed a nanoplatform capable of overcoming biological barriers for synergistic chemo-photothermal therapy. As illustrated in Scheme 1, HA was grafted onto the PPy nanoneedles through an ester linker, and then the chemotherapeutical drug doxorubicin (DOX) was conjugated to the nanoneedles *via* amidation reaction. The PPy-HA@DOX with high aspect ratios could enhance the tumbling and oscillatory effects in vasculature, reduce the steric hindrance from, and further enable extravasation (overcoming barrier 1: hemorheological flow limitations and endothelial extravasation). Subsequently, the nanoplatform transported across tumor cell membrane *via* CD44 receptor-mediated endocytosis mechanism and penetration mechanism (overcoming barrier 2: cellular internalization). Due to the high aspect ratios, PPy-HA@DOX nanoneedles were expected to enter nucleus easily *via* the nuclear pore complex by passive diffusion (overcoming barrier 3: nucleus drug delivery). More importantly, it was more than critical for PPy-HA@DOX to exploit the merits of synergistic combination of chemo-photothermal therapy. By this delicate design, the PPy-HA@DOX nanoneedles modulated their *in vivo* fate and increased the tumor accumulation by overcoming biological barriers, which held a great promise in cancer treatments.

Experimental

Synthesis of PPy-HA@DOX

PPy nanoneedles were synthesized *via* aqueous dispersion polymerization as reported.[26] Briefly, 100 mg pyrrole-3-carboxylic acid and 36 mg NaOH were dissolved to 100 mL pure water. The mixture was stirred for 1 h, then 486 mg $FeCl_3 \cdot H_2O$ was added and stirred for another 0.5 h. Then the system temperature maintained at 60 °C for 12 h. And the resulted PPy nanoneedles were obtained by centrifugation.

For HA modification, 10 mg PPy nanoneedles, 10 mg HA, 20 mg dimethylaminopyridine, 60 mg dicyclohexylcarbodiimide, 5 mL DMSO and 5 mL dichloromethane were mixed and stirred for 12 h. Then the PPy-HA was concentrated by centrifugation.

DOX loading. The DOX was conjugated to the nanoneedles *via* amidation reaction. PPy-HA was activated by EDC·HCl and NHS with molar ratio of 1 : 1 : 1 in *N*,*N*-dimethylformamide for 0.5 h. Then DOX was added to the above mixture and stirred for 24 h. As an end, the retrieved PPy-HA@DOX was collected by centrifugation. Then the free DOX collected from supernatants was quantified spectrophotometrically at 480 nm. $M_{\text{DOX-loaded}} = M_{\text{DOX-prep}} - M_{\text{DOX-free}}$. DOX loading capacity (LC) was calculated according to the following formula:

$$\text{LC} = \frac{M_{\text{Dox-loaded}}}{M_{\text{Dox-loaded}} + M_{\text{PPy-HA}}}$$

Characterization

Transmission electron microscope (TEM) and dynamic light scattering (DLS) were used to characterize the particle size and morphology of the samples. Spectrophotometry measurements were carried out on an UV-vis spectrometer (Shimadzu).

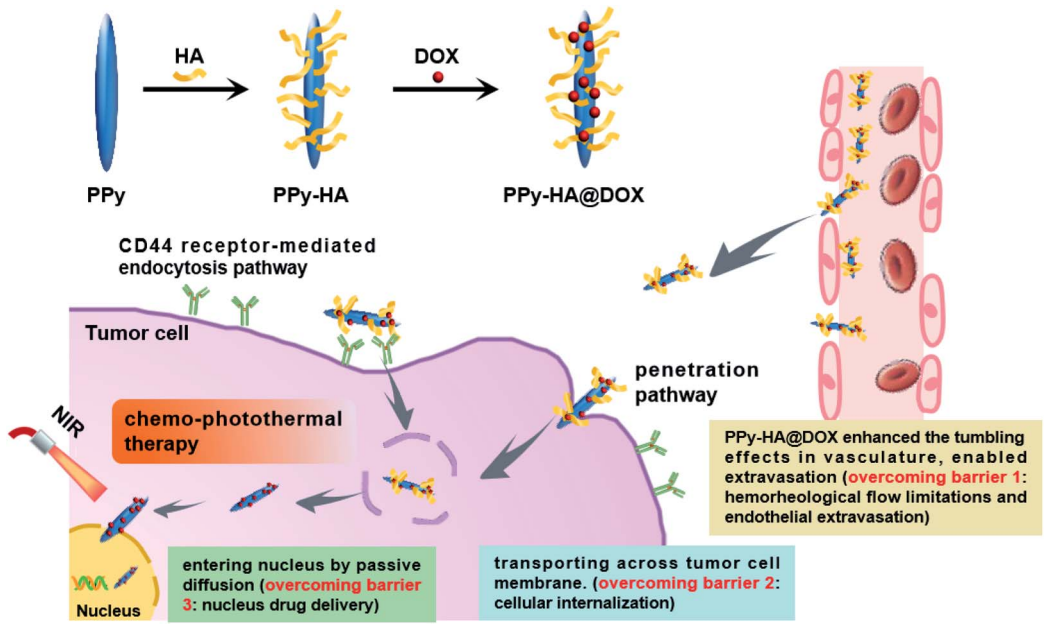

Scheme 1 Schematic illustration of PPy-HA@DOX capable of overcoming biological barriers for synergistic chemo-photothermal therapy.

FT-IR spectra were recorded on a Nicolet iS10 spectrometer (Thermo, USA).

Photothermal performance evaluation

Samples of PPy-HA@DOX with different concentrations were irradiated by an 808 nm laser at different radiant energy. The temperature changes were recorded and imaged by a thermal camera (FLIR, T330) at indicated time points.

Cellular culture

MCF-7 human breast cancer cells were obtained from Fuxiang Biotech Company, Shanghai, China. Cells were cultured in RPMI-1640 culture medium containing 10% fetal bovine serum (FBS), 0.1 mg mL^{-1} streptomycin and 100 U mL^{-1} penicillin at 37 °C in a humidified incubator of 5% (v/v) CO_2 in air.

Cellular uptake

MCF-7 cells (1.5×10^5 cells per well) were incubated with PPy@DOX, PPy-HA@DOX nanospheres or nanoneedles in normal culture medium and PPy-HA@DOX in culture medium with free HA (5 mg mL^{-1}), respectively. After a 4 h incubation, then cell nucleus were stained with DAPI for another 30 min. At last, cell imaging was conducted by using confocal laser scanning microscopy (CLSM, Olympus FV1100) after washing cells with PBS.

Cell viability measurements

MCF-7 cells were incubated with different concentrations of PPy and PPy-HA, as well as the different formulations of PPy, PPy-HA, DOX, PPy@DOX and PPy-HA@DOX (PPy concentration: 20 μg mL^{-1}, DOX concentration: 5 μg mL^{-1}), respectively. The cells were irradiated by an 808 nm laser (2 W cm^{-2}, 3 min) and then incubated for another 24 h. The cell viability was measured using MTT assay.

In vivo pharmacokinetic study

The animal procedures were performed in accordance with the Guidelines for Care and Use of Laboratory Animals of Zhengzhou University, and the experiments were approved by the Animal Ethics Committee of Zhengzhou University. The pharmacokinetics of PPy-HA@DOX nanoneedles. Briefly, the MCF-7 tumor-bearing mice were i.v. injected with DOX, PPy@DOX and PPy-HA@DOX nanoneedles ([DOX] = 4 mg kg^{-1}), respectively. Then, the peripheral blood was collected at predetermined intervals and the blood was then centrifuged at 4 °C (3000 g, 5 min) to obtain the plasma. The plasma samples were mixed with saline, 50% methanol, and $ZnSO_4$ (final concentration: 400 mg mL^{-1}) and then centrifuged. The supernatants were determined by HPLC with the following conditions: a Symmetry® C18 column; mobile phase, 50 mM sodium phosphate buffer (pH 3.0)/acetonitrile: 65/27; column temperature: 30 °C; fluorescence detector set: $\lambda_{ex} = 480$ nm and $\lambda_{em} = 550$ nm.

In vivo antitumor activity

MCF-7 tumor bearing mice were divided into 10 groups ($n = 6$). The mice were intravenous injected with saline, PPy-HA, DOX, PPy@DOX and PPy-HA@DOX ([PPy] = 16 mg kg^{-1}, [DOX] = 4 mg kg^{-1}) every other day, respectively. For the laser-treated groups, the tumors of mice were irradiated by an 808 nm laser (2 W cm^{-2}, 1 min) at 6 h after injection. The tumors were monitored calculated as $(\text{tumor width})^2 \times (\text{tumor length})/2$. When the treatments finished, tumors were removed for H&E staining.

Statistical analysis

Data were presented as mean ± standard deviation (S.D.). Statistical significance was analyzed by Student's *t* test and set at probabilities of $^*P < 0.05$, and $^{**}P < 0.01$.

Results and discussions

Synthesis of PPy-HA@DOX

The PPy nanoneedles were synthesized *via* aqueous dispersion polymerization as reported.[27] The TEM image (Fig. 1A) of PPy nanoparticles clearly showed the needles-like morphology with a length of ~40 nm and width of ~5 nm. And the dynamic light scattering analysis also indicated the particle size of 57.2 ± 2.9 nm (Fig. S1†), a little higher than the TEM results. During the synthesis procedure of PPy nanoneedles, pyrrole-3-carboxylic acid was selected as the conducting polymer monomer. The FT-IR results in Fig. 1B showed the characteristic peaks of abundant carboxyl groups (1628 cm^{-1}), which provided advantages for further modification.

The illustration of synthesis of PPy-HA@DOX was shown in Fig. S2.† For the synthesis of PPy-HA@DOX, HA was grafted onto the PPy nanoneedles through an ester linker, and then the chemotherapeutical drug doxorubicin (DOX) was conjugated to the nanoneedles *via* amidation reaction. The emerging characteristic C=O (1735 cm^{-1}) of ester linkage and the –NH–CO– peak (1654 cm^{-1}) in Fig. 1B revealed the successful HA modification and DOX loading. The TEM of the PPy-HA samples was investigated. Fig. S3† showed all the PPy nanoparticles were evidently wrapped around by high molecular polysaccharide HA. The amount of modified HA was about 9.7% in the system by using HA quantitative assay kit (up-conversion luminescence method). And the UV-vis absorption spectrum in Fig. 1C showed PPy nanoneedles showed a strong absorption in NIR region. These results were in agreement with previous reports,[15–17] suggesting the potential photothermal agent of PPy. In addition, PPy-HA@DOX also displayed the typical absorption peak of DOX at 480 nm, further revealing the DOX loading (17.2%, mass ratio).

In the initial stage of synthesis of PPy nanoneedles, massive Py-3-COOH radical cations and Fe^{2+} were generated due to the chemical oxidation reaction between Py-3-COOH and $FeCl^{3+}$. Then needle-like FeOOH, formed in the present of NaOH and Fe^{2+}, subsequently acted as a morphology inducer in the polymerization of Py-3-COOH radical cations, leading to the fabrication of PPy nanoneedles. So the PPy nanoneedles had

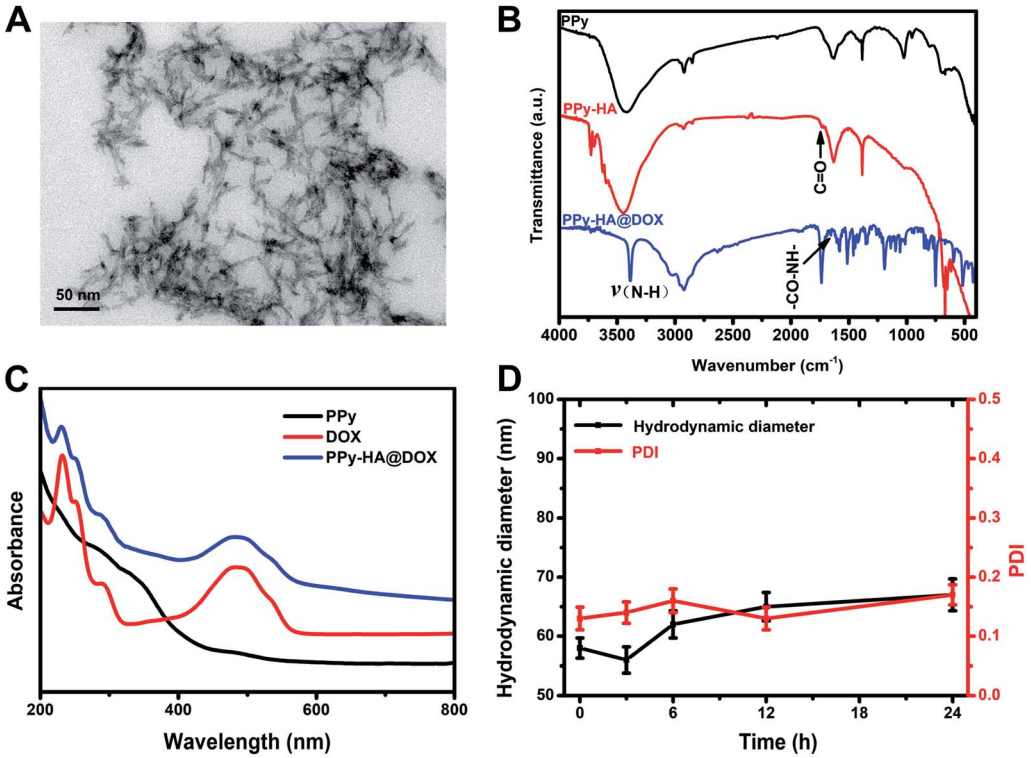

Fig. 1 Characterization of PPy-HA@DOX. (A) TEM image of PPy. (B) FT-IR spectra. (C) UV-vis absorption spectra. (D) Colloidal stability of PPy-HA@DOX in cell culture medium containing 10% fetal bovine serum over 24 h.

abundant COOH group and showed positive zeta potential (39.5 ± 6.4 mV). Then HA with –OH groups was grafted onto the PPy nanoneedles through an ester linker, and then DOX with $-NH_2$ groups was conjugated to the nanoneedles *via* amidation reaction. After HA coating and DOX loading, the zeta potential of the nanoneedles was −29.7 ± 1.8 mV and −22.9 ± 2.3 mV (Fig. S4†), respectively. And the negative charge of PPy-HA@DOX was conducive to individual dispersion and long blood circulation property of the nanoparticles.[31] As reported by some literature, the *in vivo* behavior of nano system was influenced by the surface properties such as zeta potential.[20] Positively charged particles could facilitate tumor penetration. However, they normally led to unspecific protein adsorption on cationic particles, while protein-loaded particles could be quickly removed by the immune system. In contrast, negatively charged particles increased the circulation time in blood.[29] Additionally, HA modification could improve the hydrophilicity of PPy, which was useful to prevent opsonization reaction and prolong blood circulation half-life.[3] The *in vivo* pharmacokinetics study was investigated (Fig. S5†). DOX from the solution was cleared rapidly from the blood. On the contrary, PPy@DOX and PPy-HA@DOX nanoneedles exhibited a delayed blood clearance. In addition, DOX level from the PPy-HA@DOX remained higher at all time points than that of PPy@DOX solution. Then the pharmacokinetic parameters were analyzed by non-compartment methods with PK solver software. The terminal half-life time of DOX, PPy@DOX and PPy-HA@DOX nanoneedles were 1.32 ± 0.31, 1.79 ± 0.38 and 1.86 ± 0.25 h, respectively. Therefore, PPy-HA@DOX with hydrophilic and negative-charged surface exhibited enhanced blood circulation to some extent.

Then the dispersibility of the system was investigated (Fig. 1D). The PPy-HA@DOX dispersion in cell culture medium remained always stable with minimal size changes over 24 h, which could be assigned to the hydrophilic character of HA. Besides,the drug release profiles at different conditions were investigated. The drug release behaviors among DOX, PPy-HA@DOX nanospheres and nanoneedles were investigated. Fig. S6† showed that the release of DOX group was very fast in buffer solution, while DOX release from PPy-HA@DOX nanospheres and nanoneedles was slow and sustained, which was benefit for the enhanced antitumor activity of DOX in tumor cells. As Fig. S7† showed, only tiny amounts increase of DOX release was observed in PPy-HA@DOX nanoneedles group under pH 6.5 and 7.4 (about 33.13% and 37.53%, respectively) within 14 h, indicating that PPy-HA@DOX did not display pH responsive drug release profile. These results were due to the fact that DOX was conjugated to the nanoneedles *via* amidation reaction.

Photothermal performance evaluation

Motivated by the strong absorption in NIR region of PPy as mentioned above, we moved on to investigate the photothermal performance. As Fig. 2A and B depicted, the temperature of PPy-HA@DOX increased rapidly under 808 nm laser irradiation, exhibited PPy concentration, NIR radiant energy and irradiation

time-dependent features. Of note, the thermal images in Fig. 2C showed the temperature of PPy-HA@DOX (100 μg mL^{-1}) increased by even 28.9 °C (from 26.4 °C to 55.3 °C) after 12 min of 808 nm laser irradiation (2 W cm^{-2}), revealing that PPy could effectively convert the 808 nm laser energy into thermal energy.[27,28] Therefore, the excellent photothermal heating effect of PPy-HA@DOX suggested it could be applied as promising photothermal agent for thermal ablation in cancer treatments.

Cellular uptake

Next, the activity of PPy-HA@DOX overcoming cellular barriers was investigated on MCF-7 (CD44 over-expressed) human breast cancer cells. The uptake and intracellular translocation of PPy-HA@DOX nanospheres and nanoneedles were observed in Fig. 3A. Based on the intrinsic specific red fluorescence of DOX, the location of PPy nanospheres was tracked by DOX loading. DAPI for nuclei staining (blue) and DOX fluorescence (red) were recorded. Compared to PPy@DOX group, both PPy-HA@DOX nanospheres and nanoneedles exhibited a stronger fluorescence in cells. Furthermore, the fluorescence intensity of DOX reduced by excess free HA in a competitive binding study. These results demonstrated the HA as the tumor targeting ligand had the high binding ability with CD44 receptor and thus could be internalized *via* receptor-mediated endocytosis.[32] It was worthwhile to note that the weak red fluorescence of nanospheres group mainly accumulated in the perinuclear cytoplasm, while the DOX in nanoneedles group was directly embedded in nucleus. Some papers had reported that the cylindrical shaped nanoparticles with a high aspect ratios had larger contact area with the cell membrane than spherical nanoparticles, which could penetrate cell membrane (similar to a "nanosyringe") by energy-independent mechanism.[25] What's more, the nonspherical particles were inclined to enter nucleus *via* the nuclear pore complex by passive diffusion.[26] In this sense, the PPy-HA@DOX nanoneedles were capable of accumulating in the nucleus effectively and overcoming cellular barriers (cellular internalization and nuclear drug delivery), which was expected to exhibit much higher cytotoxicity to tumor cells.

Cell viability measurements

In vitro cytotoxicity was then investigated on MCF-7 cells. Before that, the biocompatibility of PPy nanoneedles was evaluated. Fig. 3B showed that no obvious changes in cell viability were found after treatments with PPy and PPy-HA nanoneedles, even at a high concentrations (500 μg mL^{-1}). These results indicated the excellent biocompatibility of PPy for biological applications. Then an 808 nm laser irradiation was conducted to explore the phototoxicity (Fig. 3C). Both PPy and PPy-HA nanoneedles groups induced an excellent PTT cytotoxic effect with a decreased cell viability (83.8 ± 3.7% and 74.3 ± 4.6%, respectively). And the lower cell viability of PPy-HA group could be due to the higher cellular internalization of HA modified nanoparticles. It was found that only PTT or chemotherapy could not kill cells thoroughly. In contrast, PPy-HA@DOX

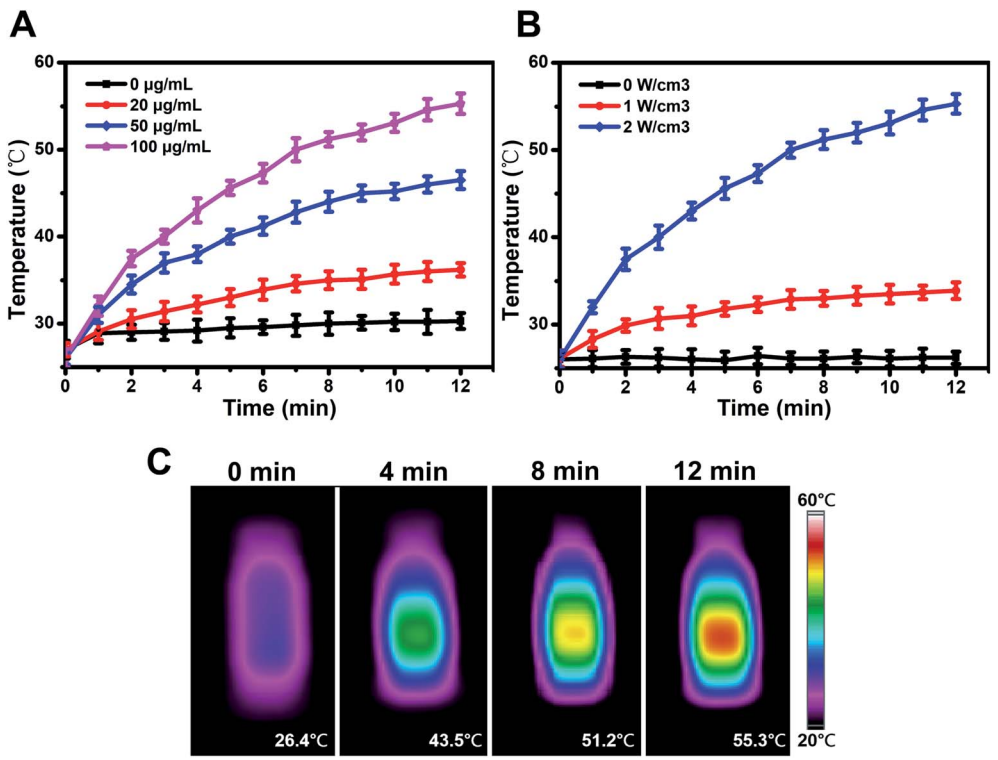

Fig. 2 (A) Temperature changes of PPy-HA@DOX with different concentrations by 808 nm laser at a power density of 2 W cm^{-2}. (B) Temperature changes of PPy-HA@DOX (100 μg mL^{-1}) at different radiant energy. (C) Thermal images of PPy-HA@DOX (100 μg mL^{-1}) after 12 min of 808 nm laser irradiation (2 W cm^{-2}).

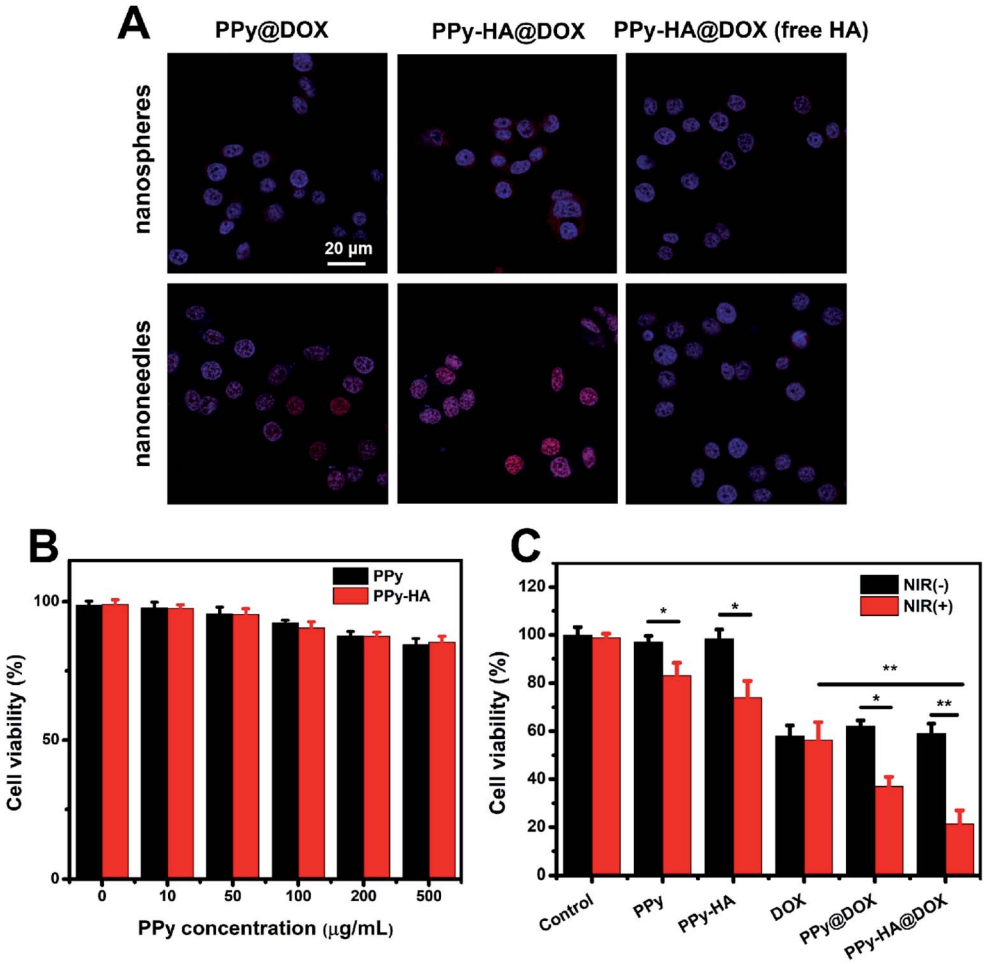

Fig. 3 *In vitro* cell experiments. (A) Cellular uptake of PPy@DOX nanoneedles, PPy-HA@DOX nanoneedles and PPy-HA@DOX nanoneedles with free HA (5 mg mL^{-1}) in MCF-7 cells. (B) Cell viability of MCF-7 cells with different concentrations of PPy nanoneedles and PPy-HA nanoneedles. (C) Cell viability of different treatments on MCF-7 cells under NIR irradiation (808 nm, 2 W cm^{-2}, 3 min).

nanoneedles + NIR group reduced the cell viability of 21.4 ± 2.9%, far lower than that of PPy-HA nanoneedles + NIR (74.3 ± 4.6%) and DOX (56.4 ± 3.1%) group. Besides, Fig. S8† showed that both PPy nanoneedles and nanospheres displayed excellent PTT effect. And there was no obvious difference in cytotoxicity between these two materials. Thus, the PPy-HA@DOX nanoplatform showed an excellent synergetic combination of chemo-photothermal therapy. And the shape effect of PPy nanoneedles for overcoming biological barriers should be responsible for this high therapeutic efficacy.

In vivo antitumor activity

Followed by the *in vitro* experiments of the nanoplatform, we then explored the feasibility in MCF-7 tumor-bearing nude mice. The confocal microscopy images clearly indicated the DOX distribution in tumor site (Fig. 4A). Compared to the nanospheres group, the PPy-HA@DOX nanoneedles group showed a wide and evident fluorescence throughout the tumor region. The anti-CD31 immunohistochemical staining (green, tumor vasculature marker) showed there was no significant differences in vascular density. In addition, the fluorescence imaging *in vivo* of PPy-HA@DOX@IR783 nanoneedles and PPy-HA@DOX@IR783 nanospheres were investigated. Fig. S9† showed that the elevated fluorescence signals of PPy-HA@DOX@IR783 nanoneedles mainly concentrated on the tumor tissue in comparison with PPy-HA@DOX@IR783 nanospheres. These results indicated that the nanoneedles showed a superior tumor targeting effect. These results could be assigned to the fact that the nanoneedles with high aspect ratios exhibited seriously lateral drift, the unique tumbling and margination dynamics, which potentiated the propensity of nanoparticle-endothelial cell wall contact and then enhanced the extravasation through the fenestrated vasculature of tumors.[20] Subsequently, the infrared thermal imaging was conducted *in vivo* (Fig. 4B). It was found that the temperature of tumor increased from 34.5 °C to 48.3 °C after 150 s NIR irradiation in PPy-HA@DOX nanoneedles group, which exceeded the damage threshold. What's more, the PPy-HA@DOX nanospheres group was also investigated. As shown in Fig. S10,† the temperature of tumor increased from 34.8 °C to 44.5 °C after 150 s NIR irradiation, lower than that of PPy-HA@DOX nanoneedles. The superior photothermal effect of nanoneedles than

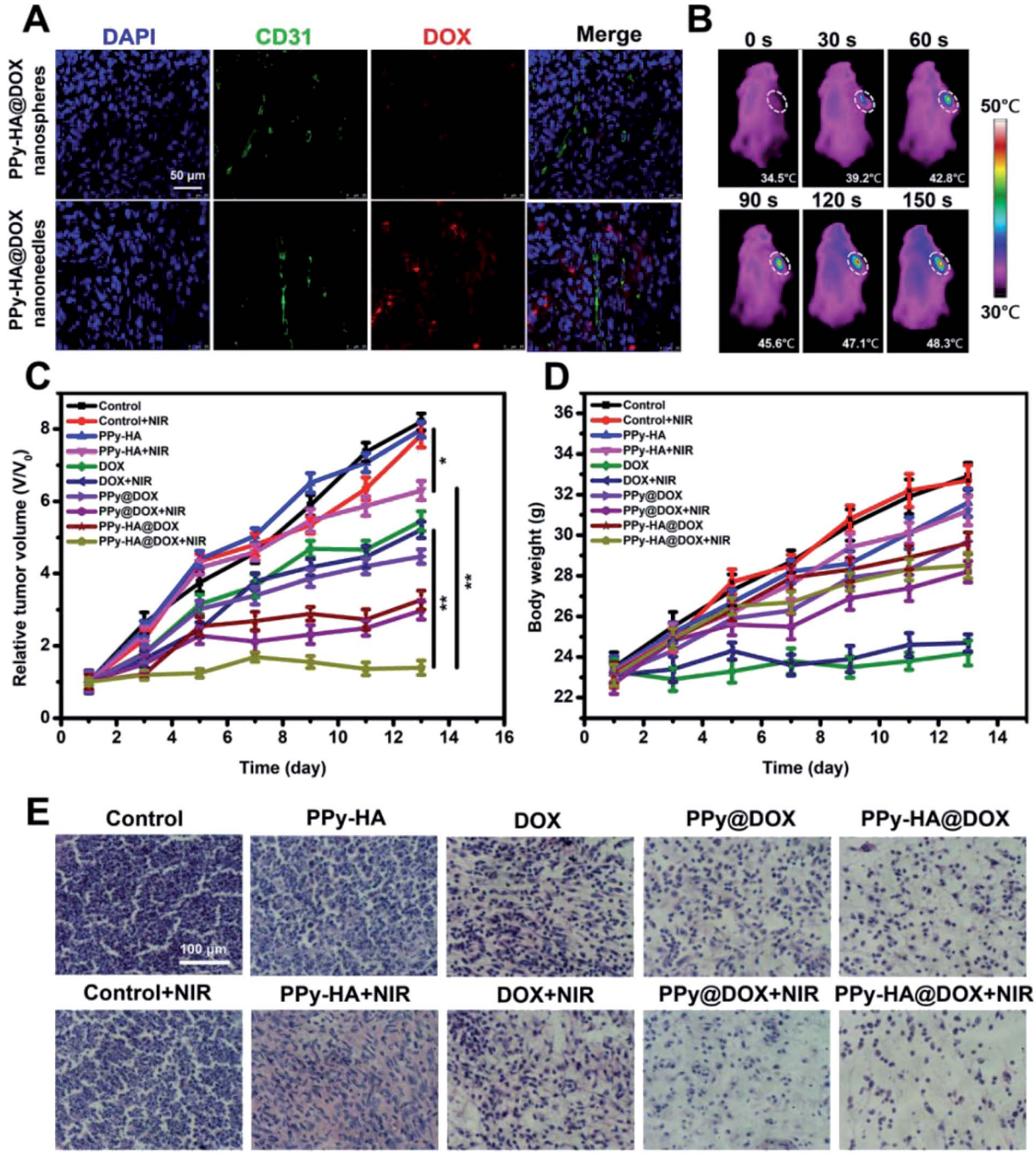

Fig. 4 *In vivo* experiments. (A) *Ex vivo* fluorescence images of tumors. The vessels were stained with anti-CD34 antibody (green). (B) Thermal images of tumor-bearing mice after injection of PPy-HA@DOX nanoneedles under NIR irradiation (808 nm, 2 W cm^{-2}). (C) Tumor volume changes of mice after different nanoneedles treatments. (D) Body weight changes of mice in (C). (E) H&E stained tumors obtained from different treatment groups in (C).

nanospheres could be ascribed to the superior tumor targeting efficiency of nanoneedles.

Then *in vivo* antitumor effect was assessed in MCF-7 tumor-bearing mice. The relative tumor volumes for each group as a function of time were plotted in Fig. 4C. The mice treated with NIR laser alone or PPy-HA nanoneedles without NIR irradiation displayed rapidly increasing tumor volumes and did not show any therapeutic effect. After NIR irradiation, PPy-HA nanoneedles resulted in a moderate inhibition of tumor growth with V/V_0 of 6.30 ± 0.26. The tumor bearing mice treated with DOX, PPy@DOX nanoneedles and PPy-HA@DOX nanoneedles achieved V/V_0 of 5.21 ± 0.23, 4.47 ± 0.19 and 3.27 ± 0.29, respectively, showing the substantial therapeutic effect. However, the tumor could not be regressed by these methods unfortunately. Then PPy-

HA@DOX nanoneedles was injected and exposed to NIR irradiation in order to obtain higher anti-tumor efficacy. Attractively, remarkably enhanced anti-tumor efficacy based on chemo-photothermal therapy was observed with V/V_0 of 1.39 ± 0.20 as previously expected in cell culture system. Besides, the PPy-HA@DOX nanospheres groups were also assess their activity. As Fig. S11† showed, the tumor bearing mice treated with PPy-HA@DOX nanospheres with NIR irradiation achieved V/V_0 of 1.96 ± 0.23, which displayed worser antitumor effect than PPy-HA@DOX nanoneedles groups. The higher antitumor activity of nanoneedles might be ascribed to the ability of overcoming biological barriers, which was benefit for enhanced chemo-photothermal therapy. In addition, the histology study of tumors was carried out (Fig. 4E). Compared with the control group, PPy-HA@DOX nanoneedles + NIR group displayed a large amount of apoptosis pathological characteristics. Such excellent therapeutic effect of PPy-HA@DOX nanoneedles could be due to the ability of overcoming biological barriers for synergistic chemo-photothermal therapy.

The toxicity of nanoparticles should be taken into consideration before their clinical application. The no abnormalities in body weight demonstrated that PPy-HA nanoneedles was a safe carrier as expected (Fig. 4D). Histological tissue images in major organs through H&E staining was shown in Fig. S12.† It was clear to see that free DOX induced cardiac muscle fiber breakage and heart cell nucleus gather due to its cardiotoxicity, while no lesions were detected in PPy-HA@DOX. These results indicated the tumor-targeted PPy-HA@DOX nanoneedles might decrease the DOX level in normal tissues and could reduce toxic side effects as well as improve the therapeutic index of DOX to a certain extent. HA coating could protect the PPy from external environment, thus dramatically improving the stability and biocompatibility of the system. The pathological characteristics of each tissue in PPy-HA group were normal as these in control group, which suggested that PPy-HA exhibited good biosafety and could be employed as a promising drug carrier.

Conclusions

In summary, this work developed a nanoplatform (PPy-HA@DOX) capable of overcoming biological barriers for synergistic chemo-photothermal therapy. Both *in vitro* and *in vivo* experiments demonstrated that PPy-HA@DOX nanoneedles with high aspect ratios could enable extravasation, enhance the cellular internalization *via* CD44 receptor-mediated endocytosis mechanism and penetration mechanism, and enter nucleus easily *via* the nuclear pore complex by passive diffusion. Possessing the ability of overcoming biological barriers, the PPy nanoneedle based nanoplatform exploited the merits of synergistic combination of chemo-photothermal therapy, which would pave the way toward more effective nanotherapeutics.

Conflicts of interest

There are no conflicts to declare.

Acknowledgements

The work is supported by grants from Xinxiang Medical University Doctoral Research Start Fund (505267), Key Scientific Research Project of Colleges and Universities in Henan Province (15A310008).

References

1 Y. J. Liu, P. Bhattarai, Z. F. Dai and X. Y. Chen, *Chem. Soc. Rev.*, 2019, **48**, 2053–2108.
2 Q. Chen, Q. Y. Hu, E. Dukhovlinova, *et al.*, *Adv. Mater.*, 2019, **31**, 1900192.
3 Q. H. Feng, W. X. Zhang, X. M. Yang, *et al.*, *Adv. Healthcare Mater.*, 2018, **7**, 1700957.
4 Q. Feng, Y. Zhang, W. Zhang, *et al.*, *Acta Biomater.*, 2017, **49**, 402–413.
5 F. F. Zhao, J. Zhou, X. J. Su, *et al.*, *Small*, 2017, **13**, 1603990.
6 J. Zhou, P. Luo, C. Sun, *et al.*, *Nanoscale*, 2017, **9**, 4244–4254.
7 H. S. Jung, P. Verwilst, A. Sharma, *et al.*, *Chem. Soc. Rev.*, 2018, **47**, 2280–2297.
8 B. Du, S. P. Han, H. Y. Li, *et al.*, *Nanoscale*, 2015, **7**, 5411–5426.
9 X. J. Su, F. F. Zhao, Y. H. Wang, *et al.*, *Nanomedicine*, 2017, **13**, 1761–1772.
10 Q. H. Feng, W. X. Zhang, Y. Z. Li, *et al.*, *Nanoscale*, 2017, **9**, 15685–15695.
11 Y. Y. Yin, L. L. Cui, F. L. Yan, *et al.*, *J. Mater. Chem. B*, 2017, **5**, 454–463.
12 L. Wang, J. J. Shi, Y. W. Hao, *et al.*, *J. Biomed. Nanotechnol.*, 2015, **11**, 1653–1661.
13 X. Chen, X. F. Zhu, T. Y. Xu, *et al.*, *J. Mater. Chem. B*, 2019, **7**, 112–122.
14 H. H. Ye, X. Li, L. Deng, *et al.*, *Ind. Eng. Chem. Res.*, 2019, **58**, 3269–3281.
15 X. X. Bi, H. L. Su, W. Shi, *et al.*, *J. Mater. Chem. B*, 2018, **6**, 7877–7888.
16 K. Yang, H. Xu, L. Cheng, *et al.*, *Adv. Mater.*, 2013, **25**, 945.
17 X. Wang, Y. C. Ma, X. Sheng, Y. C. Wang and H. X. Xu, *Nano Lett.*, 2018, **18**, 2217–2225.
18 D. Yan, X. Liu, G. Deng, *et al.*, *J. Colloid Interface Sci.*, 2018, 530.
19 R. Xu, G. D. Zhang, J. H. Mai, *et al.*, *Nat. Biotechnol.*, 2016, **34**, 414–418.
20 E. Blanco, H. Shen and M. Ferrari, *Nat. Biotechnol.*, 2015, **33**, 941–951.
21 V. P. Chauhan and R. K. Jain, *Nat. Mater.*, 2013, **12**, 958–962.
22 X. L. Huang, X. Teng, D. Chen, F. Q. Tang and J. Q. He, *Biomaterials*, 2010, **31**, 438–448.
23 V. P. Chauhan, Z. Popovic, O. Chen, *et al.*, *Angew. Chem., Int. Ed.*, 2011, **50**, 11417–11420.
24 P. Kolhar, A. C. Anselmo, V. Gupta, *et al.*, *Proc. Natl. Acad. Sci. U. S. A.*, 2013, **110**, 10753–10758.
25 J. Yang, Y. P. Wu, Y. Shen, *et al.*, *ACS Appl. Mater. Interfaces*, 2016, **8**, 26578–26590.
26 E. Hinde, K. Thammasiraphop, H. T. Duong, *et al.*, *Nat. Nanotechnol.*, 2017, **12**, 81–89.

27 X. Liu, H. L. Su, W. Shi, *et al.*, *Biomaterials*, 2018, **167**, 177–190.
28 Y. Wang, Y. Xiao and R. K. Tang, *Chem.–Eur. J.*, 2014, **20**, 11826–11834.
29 L. Zhang, P. Y. Hao, D. J. Yang, *et al.*, *J. Mater. Chem. B*, 2019, **7**, 953–964.
30 L. Wang, Y. J. Hu, Y. W. Hao, *et al.*, *J. Controlled Release*, 2018, **286**, 74–84.
31 Q. Feng, Y. Zhang, W. Zhang, *et al.*, *Acta Biomater.*, 2016, **38**, 129–142.
32 K. Y. Choi, G. Saravanakumar, J. H. Park and K. Park, *Colloids Surf., B*, 2012, **99**, 82–94.